

Article

# Simulation of Electromagnetic Generator as Biomechanical Energy Harvester

Nedunchelien Gurusamy <sup>1</sup>, Irraivan Elamvazuthi <sup>1,\*</sup>, Norashikin Yahya <sup>1</sup>, Steven Su <sup>2</sup> and Bao-Huy Truong <sup>3</sup>

<sup>1</sup> Department of Electrical & Electronic Engineering, Universiti Teknologi Petronas, Bandar Seri Iskandar 32610, Malaysia; nedun\_g03398@utp.edu.my (N.G.); norashikin\_yahya@utp.edu.my (N.Y.)

<sup>2</sup> School of Biomedical Engineering, University of Technology Sydney (UTS), Ultimo, NWS 2207, Australia; steven.su@uts.edu.au

<sup>3</sup> Institute of Engineering and Technology, Thu Dau Mot University, Thu Dau Mot VN-57, Vietnam; truonghoangbaohuy@tdmu.edu.vn

\* Correspondence: irraivan\_elamvazuthi@utp.edu.my

**Featured Application:** The output of this research by means of energy harvesting through biomechanical motion has the potential to be applied to charging portable devices.

**Abstract:** Portable electronic devices are dependent on batteries as the ultimate source of power. Irrefutably, batteries only have a limited operating period as they need to be regularly replaced or recharged. In many situations, the power grid infrastructure is not easily accessible to recharge the batteries and the recharging duration is also not convenient for the user to wait. Enhancement of a reliable electronic system by preventing power interruptions in remote areas is essential. Similarly, modern medical instruments and implant devices need reliable, almost maintenance-free power to ensure they are able to operate in all situations without any power interruptions. In this paper, the small-sized electromagnetic generator was designed to produce higher power by utilizing the knee angle transition involved during the walking phase as the input rotary force. The proposed generator design was investigated through COMSOL Multiphysics simulation. The achieved output RMS power was in the range of 3.31 W to 14.95 W based on the RPM range between 360 RPM to 800 RPM.

**Keywords:** gait cycle; steps; biomechanical energy harvester; knee angle; RPM; generated power



**Citation:** Gurusamy, N.; Elamvazuthi, I.; Yahya, N.; Su, S.; Truong, B.-H. Simulation of Electromagnetic Generator as Biomechanical Energy Harvester. *Appl. Sci.* **2022**, *12*, 6197. <https://doi.org/10.3390/app12126197>

Academic Editors: Gang Lei, Jianguo Zhu, Youguang Guo and Yujiao Zhang

Received: 16 May 2022

Accepted: 10 June 2022

Published: 18 June 2022

**Publisher's Note:** MDPI stays neutral with regard to jurisdictional claims in published maps and institutional affiliations.



**Copyright:** © 2022 by the authors. Licensee MDPI, Basel, Switzerland. This article is an open access article distributed under the terms and conditions of the Creative Commons Attribution (CC BY) license (<https://creativecommons.org/licenses/by/4.0/>).

## 1. Introduction

One of the difficult challenges confronting human civilization today is energy demand, of which 70% to 80% is currently met through fossil fuels [1]. Current and emerging renewable and energy-harvesting systems such as solar, wind, hydroelectric, geothermal, ocean, wave, and hydrogen are opening new possibilities that offer viable alternatives in the quest for low-carbon and non-fossil fuel energy generation. Various research has been carried out to optimize the output of these technologies [2–5].

Energy harvesting is another type of renewable energy source which has attracted researchers to pursue this in view of the global demand for portable electronic devices which continues to grow, and this has directly increased the need for wireless electrical power [6–10]. The expanding usage of portable electronic devices with small power requirements and wireless technology for modern medical devices has increased concern about the present technology of the conventional battery due to its limited lifespan and dimension. It has always been dominated by the battery size and capacity in determining the dimension, lifespan, and abilities of an electronic system [11]. These limitations have inspired many researchers to investigate energy harvesting as a potential energy source.

Energy harvesting has gained research momentum in powering up electronic devices as it has the potential to generate power for a longer lifespan. These energy resource devices are constructed in a way to operate with very minimal maintenance time or almost nearly zero maintenance and are able to operate for a longer lifespan. Energy harvesting is commonly implemented as an additional energy resource to a main power source element to further optimize the system's reliability without power interruptions. Energy generation from solar light, radio frequency, mechanical motion, and temperature variation has been demonstrated to be a feasible replacement for the conventional batteries for low-power portable electronic devices such as wearable electronics and wireless sensor networks. Technology advancements in sensor-based energy harvesting systems and energy-efficient harvesting components have driven the growth of the global market. Figure 1 shows the global energy harvesting market value and projection.

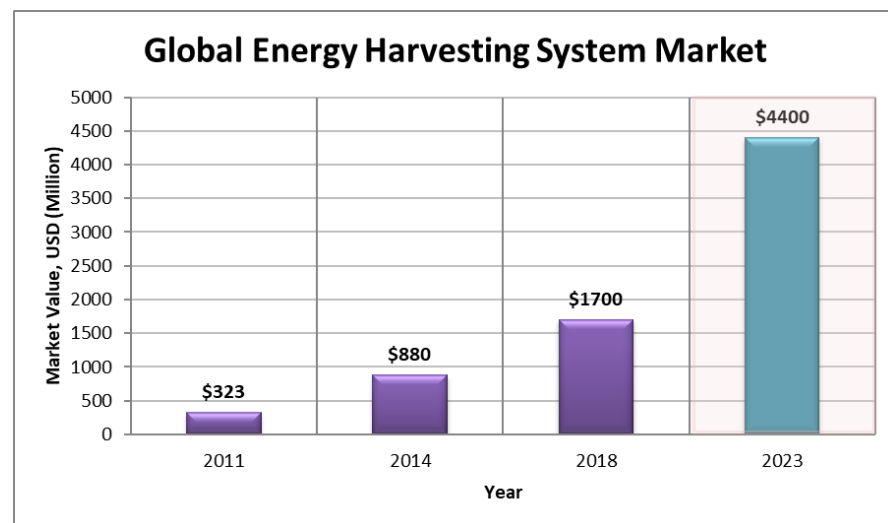


Figure 1. Global energy-harvesting market.

BCC Research through their survey report stated the global energy-harvesting system market was valued to be \$323 million in 2011 [12], \$880 million in 2014 [13], and \$1.7 billion in the year 2018. This recorded more than 5 times of growth in 7 years. The global energy-harvesting system market value is projected to be more than double by the year 2023, which is \$4.4 billion. This is equivalent to a compound annual growth rate (CAGR) of 20.2% from 2018 to 2023 [14].

Apart from energy generated from solar light, radio frequency, mechanical motion, and temperature changes, biomechanical energy harvesting is also another field with vast opportunities to replace conventional batteries. Through every single heartbeat to motion, human beings continuously dissipate energy. It's a norm for the human muscles to transform the calorie intake from food to mechanical work. The efficiency of this conversion is stated as 25% [15]. Many devices have been developed to utilize the human energy capacity in generating electrical power such as hand-crank generators, wind-up flashlights, and wristwatches [16]. The drawback of these conventional methods is the users must concentrate on the power-generating activities and this frequently results in short periods of focus. A longer duration of energy harvesting activity is only possible by harvesting the energy from everyday activities, and this will be possible by attaching the energy-harvesting device to any of the human's anatomical joints. One of the most suitable examples of this approach is the self-winding watch, where the arm movement was occupied to generate electrical power of 5  $\mu$ W [17]. Rome et al. [18,19] investigated an energy harvester by using a backpack. This backpack mechanism uses its weight as a source to initiate the rotary system attached to it and apart from the weight the output is significantly influenced by the walking speed. A total of 7.4 W was generated from this

energy harvester backpack with 38 kg as the load. Donelan et al. [20] designed a knee energy-harvester device which is 1.6 kg. At a walking speed of 1.5 m/s, the device was able to generate 3.5 W.

The lower extremity of the human is identified to be the anatomical part that exhibits higher motion during a walking gait cycle [21]. A lot of studies had been carried out to investigate the potential of energy harvesting via hip, knee, ankle, and heel strike. Feng Qian et al. [22] demonstrated two types of piezoelectric footwear harvesters with different piezoelectric stack quantities. This was designed to amplify the transferred heel strike force via force amplification frames. The average power generated at 4 km/h by the eight-stack piezoelectric is 6 mW/shoe and the six-stack piezoelectric produces 8 mW/shoe. Mustafa Ilker et al. [23], established a piezoelectric patch by optimizing the placement around the knee by using the MEMS-based piezoelectric. During walking, the harvester generated RMS power of 6.2  $\mu$ W and 12  $\mu$ W while running. Yiming Lei et al. [24] analyzed a microelectromagnetic energy harvester by converting vibration energy to electrical power. This harvester utilizes a planar copper spring mechanism and generates maximum power of 205.38  $\mu$ W at 124 Hz resonance frequency. Muhammad Toyabur Rahman et al. [25] investigated a hybridized generator by incorporating a nonlinear electromagnetic generator and triboelectric nanogenerators. This hybridized harvester generated 131.4 mW as the maximum output power during horizontal handshaking. Longhan Xie et al. [26] developed a flexible lower limb exoskeleton which is worn in parallel to assist walking gait while generating power. At the 5.1 km/h walking speed, the harvester generates a maximum power of 6.47 W. Collier Apgar et al. [27] use a brushless DC motor as the generator by integrating a gear train with a 1:86 ratio. At 5211 RPM, the generator produces 8.43 W. Jun Fan et al. [28] investigated a knee-mounted harvester with a cable-pulley mechanism. This cable-pulley mechanism converts the flexion and extension gait cycle of the knee to electrical power. This harvester generates average power of 4.1 W.

The discussed related work shows two main types of generator mechanisms which are the piezoelectric and electromagnetic generators. However, the generated power for piezoelectric ranged between 6.2  $\mu$ W and 8 mW, and electromagnetic generators ranged between 205.38  $\mu$ W and 8.43 W. This power is significantly lower, although Collier Apgar et al. [27] has produced 8.43 W at 5211 RPM which is considered better than previous work.

With these limitations, hence, in this paper, an electromagnetic generator for a biomechanical energy harvester for knee motion has been investigated and designed to produce a higher output power at lower RPM based on biomechanical motion. The proposed design is small-scale and lightweight to ensure minimal impact against the normal gait cycle of the user. As such, the proposed design is 40 mm in diameter and 10 mm in thickness. The designed small-scale generator is able to generate higher output power which is 14.95 W per device at 800 RPM with minimal effort from the user. The effort to actuate the generator is minimized by reducing the cogging torque of the generator by lowering the slot opening to slot pitch ratio. This is the major contribution of the research.

The rest of the paper is organized as follows: Section 2 focuses on electromagnetic generator modelling. Section 3 shows the simulation results and discussions with results validation through two case studies. Finally, in Section 4, the conclusion is presented.

## 2. Electromagnetic Generator Modelling

The electromagnetic generator modelling process of a single-phase permanent magnet generator involves several stages including finite element method (FEM) simulations. To limit the verification of the generator topology variations, the decision is made to consider a specific type of generator. The proposed design has 8 slots and 8 poles. The overall design process is summarized in the flowchart shown in Figure 2.

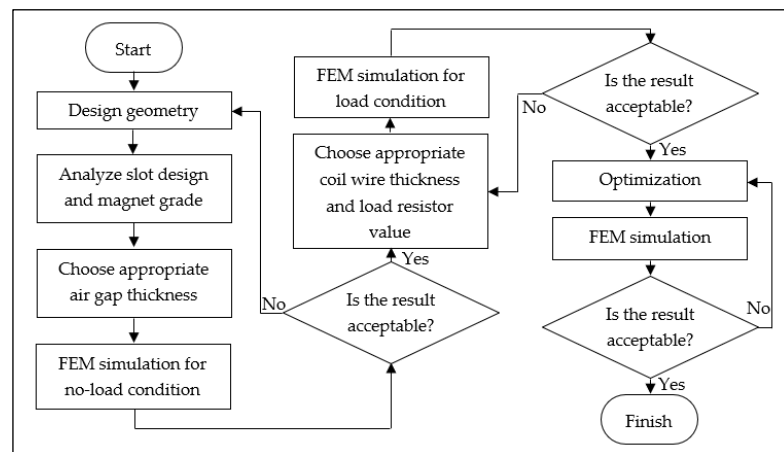


Figure 2. Electromagnetic generator design flowchart.

The initial stage involves the generator geometry, slot opening design, magnet grade, and choosing the air gap thickness. The second stage focused on coil features and load conditions. The design optimization process is the final stage.

### 2.1. Geometry of Electromagnetic Generator

In this study, an 8-slot/8-pole surface-mounted permanent magnet generator will be evaluated. The electromagnetic generator’s assembly is shown in Figure 3.

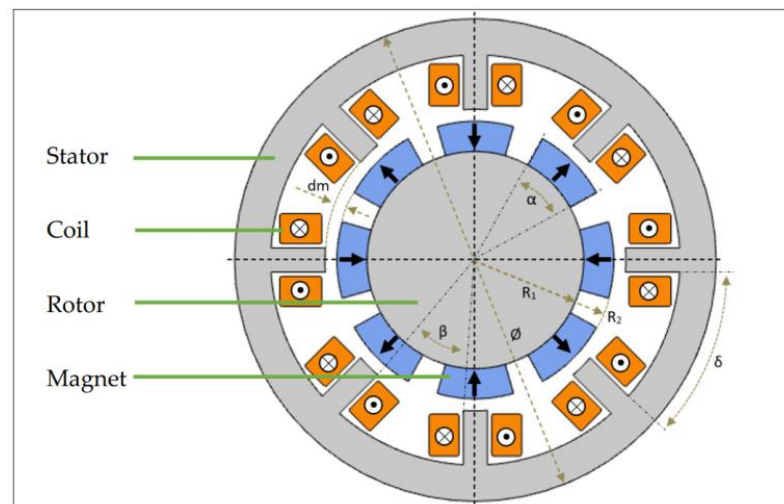
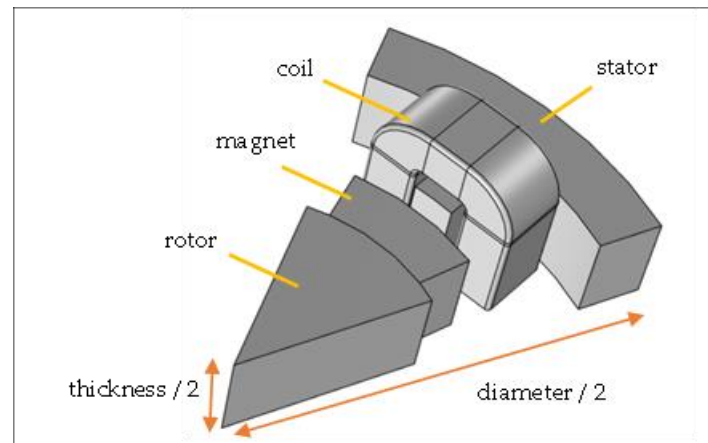


Figure 3. 2D cross-section of generator assembly.

The generator geometry represents a single-phase permanent magnet generator and the geometrical parameters are the inner radius of rotor  $R_1$ , radius of the permanent magnet surface  $R_2$ , overall diameter of generator  $\phi$ , the permanent magnet sector angle  $\alpha$ , slot pitch angle  $\delta$ , slot opening angle  $\beta$ , and the air gap thickness  $dm$ . The arrow on the permanent magnet indicates the inbound and outbound arrangement of the magnets. The dot and cross symbol on the coil represents the current flow direction in the coil. Figure 4 shows the 3D geometry view for one sector of the generator.



**Figure 4.** One sector of electromagnetic generator assembly.

The complete design of electromagnetic generator assembly will consist of 8 sectors. The assembly portion which accommodates the coil will act as a stator and the assembly holding up the magnets will act as a rotor. The permanent magnets are arranged in a sequence where it has an opposite pole from the magnets on both sides. The generator has been designed such that for every rotation of 22.5 degrees, it will change the magnetic field of the electromagnetic generators simultaneously and generate the needed electrical power. All the parameters associated with the generator are tabulated in Table 1.

**Table 1.** Parameters associated with the generator design.

Symbol	Description
S	Number of slots
P	Number of poles
$R_1$	Inner radius of the rotor
$R_2$	Permanent magnet surface radius
$\varnothing$	Overall diameter
$\alpha$	Permanent magnet sector angle
dm	Air gap thickness
$\beta$	Slot opening angle
$\delta$	Slot pitch angle
$\beta/\delta$	Slot opening to slot pitch ratio
L	Thickness
d	Coil wire diameter

## 2.2. Air Gap Thickness of the Generator

The air gap thickness between the stator and rotor needs to be determined in order to obtain the desired performance of the generator. Equation (1) shows the air gap thickness influence on the magnetic flux density in the air gap region:

$$\Phi = \text{MMF} \times (\mu_m A / \text{dm}) \quad (1)$$

where  $\Phi$  is the flux in the air gap, MMF is the magnetomotive force,  $\mu_m$  is the permeability of the magnetic material, A is the cross-sectional area, and dm is air gap thickness.

To determine the optimum air gap thickness of the generator design, the electromagnetic force reaction on the stator iron was evaluated by varying the air gap thickness between the permanent magnet and the stator iron for multiple magnet sizes as shown in Table 2 and stator designs which are square edge and T shape. Figure 5 shows the electromagnetic force strength towards the stator.

**Table 2.** Electromagnetic force by magnet dimensions for square edge stator.

Label	Magnet Size (mm) (Thickness × Outer Arc Length × Inner Arc Length)	Air Gap Thickness (mm)								Electromagnetic Force (N)
		0.5	1.0	1.5	2.0	2.5	3.0	3.5	4.0	
Magnet A	2.0 × 5.38 × 4.39	3.931	1.314	0.402	0.173	0.081	0.042	0.025	0.015	
Magnet B	2.5 × 5.62 × 4.39	6.831	1.387	0.426	0.225	0.099	0.054	0.035	0.020	
Magnet C	3.0 × 5.86 × 4.39	6.339	1.452	0.460	0.236	0.116	0.061	0.041	0.026	
Magnet D	2.0 × 6.14 × 5.03	6.449	1.390	0.462	0.241	0.122	0.065	0.040	0.025	
Magnet E	2.5 × 6.42 × 5.03	8.580	1.454	0.516	0.261	0.133	0.078	0.050	0.035	
Magnet F	3.0 × 6.70 × 5.03	6.985	1.550	0.568	0.285	0.147	0.091	0.056	0.038	

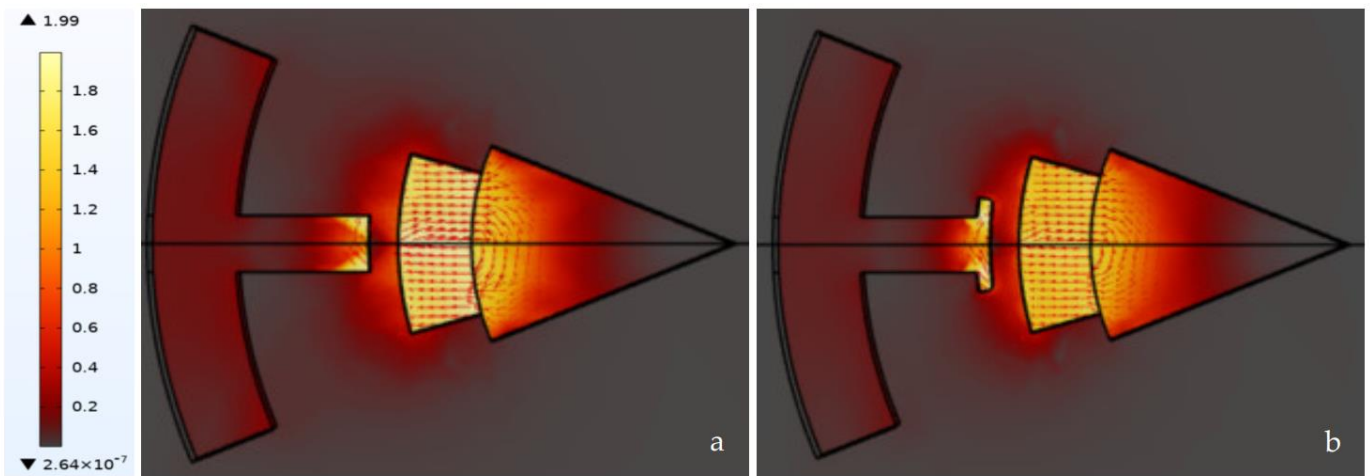


**Figure 5.** Electromagnetic force strength. (a) Square edge stator. (b) T shape stator.

The electromagnetic force strength towards the stator iron is highly influenced by the dimension of the magnet, magnetic properties, and air gap thickness. The electromagnetic force strength has been investigated for the square edge stator by varying the magnet sizes and air gap thickness as shown in Table 2.

The highest force reaction happens when the magnet is placed at a distance of 0.5 mm from stator iron. The electromagnetic force versus air gap thickness by magnet sizes has been plotted as shown in Figure 6.

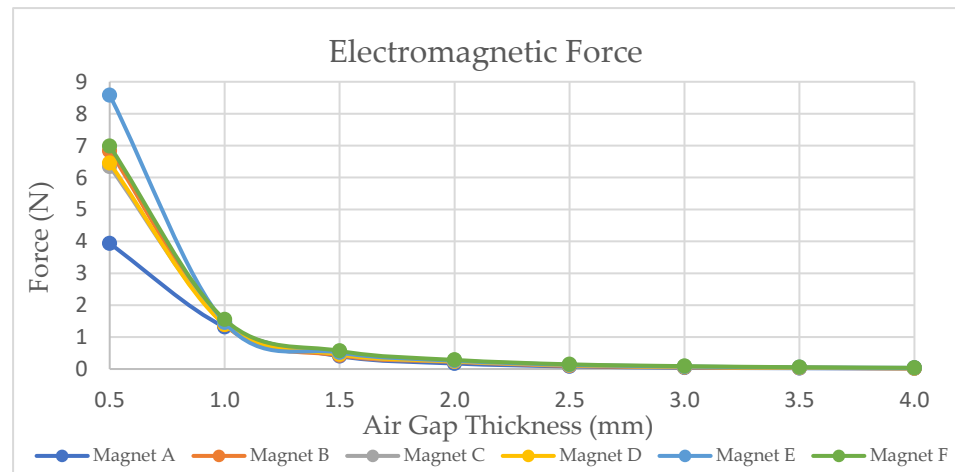


**Figure 6.** Electromagnetic force reaction due to air gap thickness by magnet size.

Because the generator is intended to be fitted into an energy-harvesting mechanism that will be worn at the hip or thigh and will be driven by leg motion, it must be designed to have minimal or zero impact on the normal gait cycle of the user. Based on Table 2, the electromagnetic force is significantly high at the 0.5 mm air gap thickness which ranges between 3.931 N and 8.58 N, and this will require a huge effort from the user to actuate the generator. Hence, the 1 mm air gap thickness is suitable for the electromagnetic generator design as it exhibits moderate electromagnetic force which ranges between 1.314 N and 1.550 N and does not require huge effort from the user.

The optimum magnet size for the electromagnetic generator is chosen based on magnetic flux density in the air gap region. Therefore, based on 1 mm air gap thickness, the magnetic flux density at air gap region was determined by varying the magnet sizes as shown in Figure 7.

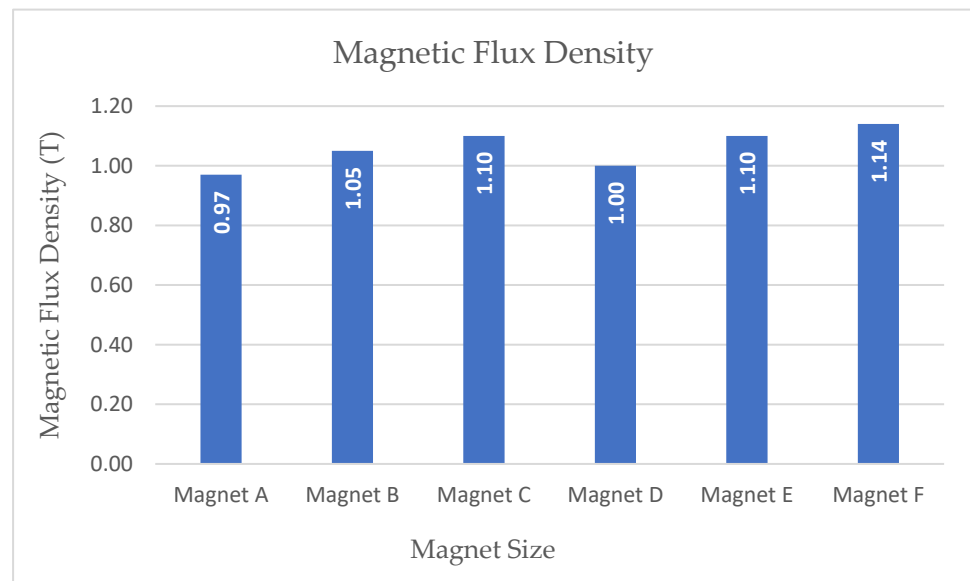


Figure 7. Magnetic flux density at the centre of the air gap region.

Magnet C, Magnet E and Magnet F demonstrate an almost similar level of magnetic flux density. Out of three magnet sizes, Magnet E is chosen for this study as the electromagnetic force is lower than Magnet F and the dimension is wider than Magnet C.

Similarly, the T shape stator is analyzed by using the Magnet E by varying the air gap thickness. Figure 8 shows the electromagnetic force and magnetic flux density for T shape stator design.

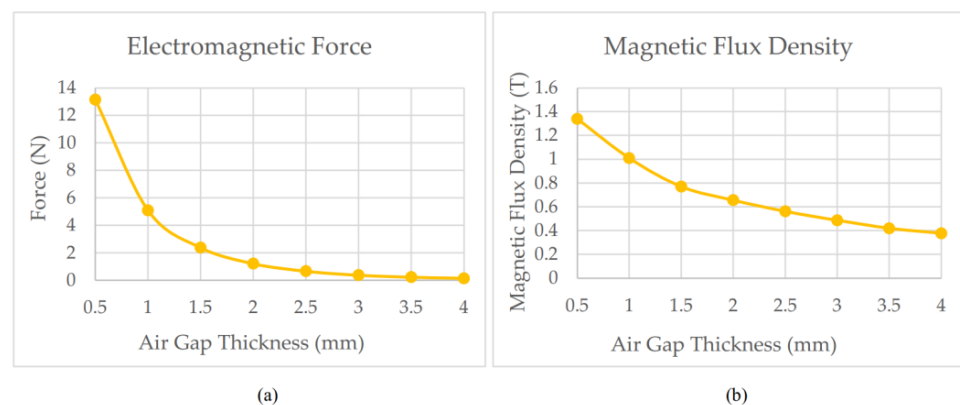


Figure 8. Reaction due to air gap thickness. (a) Electromagnetic force. (b) Magnetic flux density at the center of the air gap region.

Similar to the previous analysis, the T shape stator with 0.5 mm air gap thickness also exhibited a higher electromagnetic force which will need higher user effort. Hence, the 1 mm air gap thickness was found to be the optimum choice as the magnetic flux density is at the 1 Tesla region and other air gap thicknesses is exhibiting lower than 0.8 Tesla magnetic flux density and are not suitable for an electromagnetic generator to produce high power.

The air gap thickness of 1 mm was able to produce optimum magnetic flux density for both square edge stator and T shape stator.

### 2.3. Parameters of Electromagnetic Generator

This analysis will be based on an 8-slots/8-poles single-phase generator and the associated parameters are shown in Table 3.

**Table 3.** Parameters of electromagnetic generator.

Symbol	Description	Value	Unit
S	Number of slots	8	
P	Number of poles	8	
R <sub>1</sub>	Inner radius of the rotor	9	mm
R <sub>2</sub>	Permanent magnet surface radius	11.5	mm
Ø	Overall diameter	20	mm
α	Permanent magnet sector angle	32	°
dm	Air gap thickness	1	mm
β/δ	Slot opening to slot pitch ratio	1	
L	Thickness	10	mm
d	Coil wire diameter	AWG 24	
dm	Air gap thickness	1	mm

### 2.4. Simulation

COMSOL Multiphysics has been used to conduct the simulation work for the electromagnetic generator. This simulation is done by using the 3D rotating machinery features from COMSOL Multiphysics. There are some key simulation parameters used to carry out these simulations as shown in Table 4.

**Table 4.** Key simulation parameters.

RPM	Load	Sector	Coil N-Turn	Stator and Rotor Material	Neodymium Magnet
360, 450 and 800	10 Ohm and 100 Ohm	8	600	35PN230	N52

In COMSOL Multiphysics modelling, Equations (2)–(4) are the general equations that COMSOL solves during the simulation process:

$$\text{Electromagnetism: } \nabla \times E = -\delta B / \delta t \quad (2)$$

$$\text{Ampere's law: } \nabla \times H = J + (\delta D / \Delta t) \quad (3)$$

$$\text{Maxwell's equation for time domain: } \nabla \times (\mu^{-1} \nabla \times A) = -\sigma (\delta A / \delta t) \quad (4)$$

where E is the electric field, D is the electric displacement, J is the current, H is the magnetic field intensity, B is the magnetic flux density,  $\mu$  is the material's permeability,  $\sigma$  is the material's conductivity, and A is the magnetic vector potential. In the process, to solve the Equations (2)–(4), critical information such as boundary conditions of source and destination, material properties, and material's nonlinearities are taken into consideration.

Throughout the simulations, the RPM has been varied by three different speeds at 360, 450, and 800. The load value has been varied by two conditions at 10 ohms and 100 ohms.

The number of sectors, number of coil turns, coil wire thickness, stator and rotor material plus material of the magnet are the same.

### 3. Results and Discussion

The radial component of the magnetic flux density at the center region of the air gap under the no-load condition is shown in Figure 9.

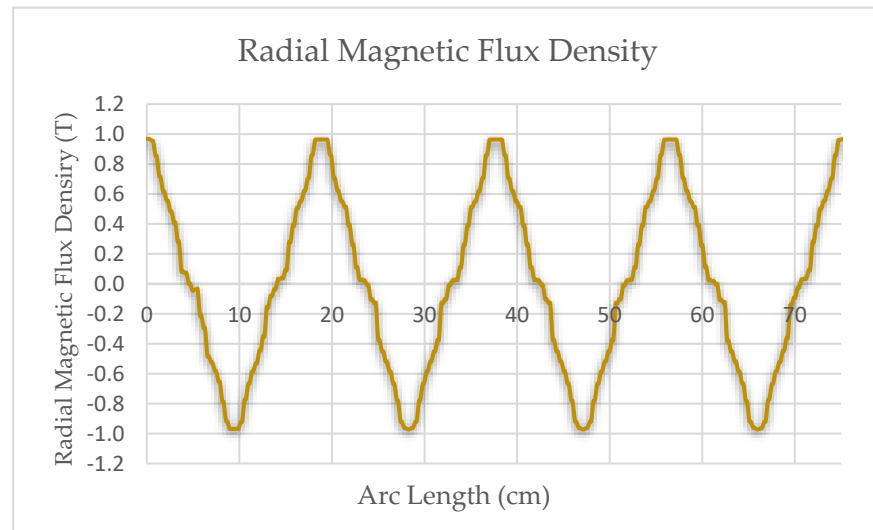


**Figure 9.** Radial magnetic flux density waveform at center of air gap.

The radial magnetic flux waveform shows a very mild distortion at the region of slots opening. The open-circuit voltage of the generator has been evaluated to analyze the waveform for the generator emf. Figure 10 shows the open circuit AC voltage of the generator.

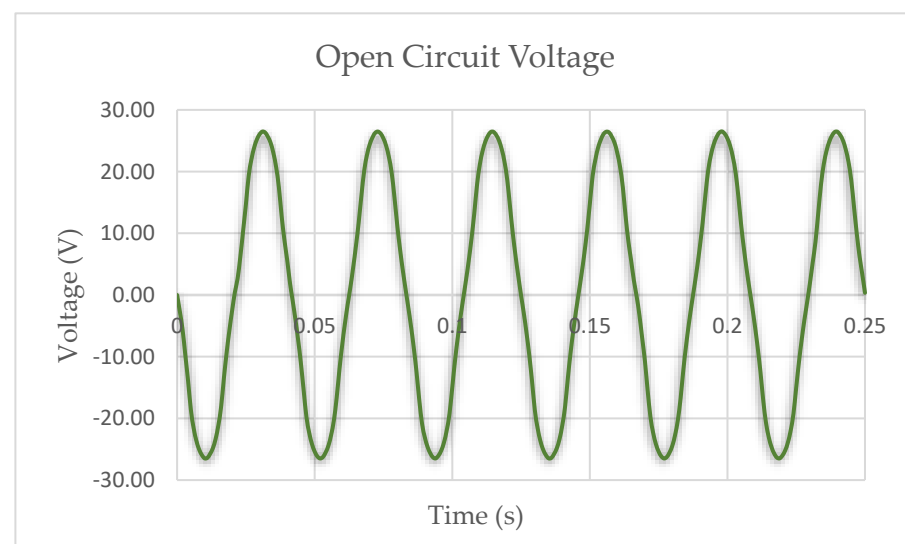


**Figure 10.** Open-circuit AC voltage.

The simulation is done for a rotation speed of 360 RPM and observed sinusoidal emf waveform for the no-load condition. This will be the basic validation to ensure there is no distortion or ripple in the voltage due to design.

Cogging torque is an important characteristic of any permanent magnet machine. The cogging torque for the proposed generator design is shown in Figure 11.

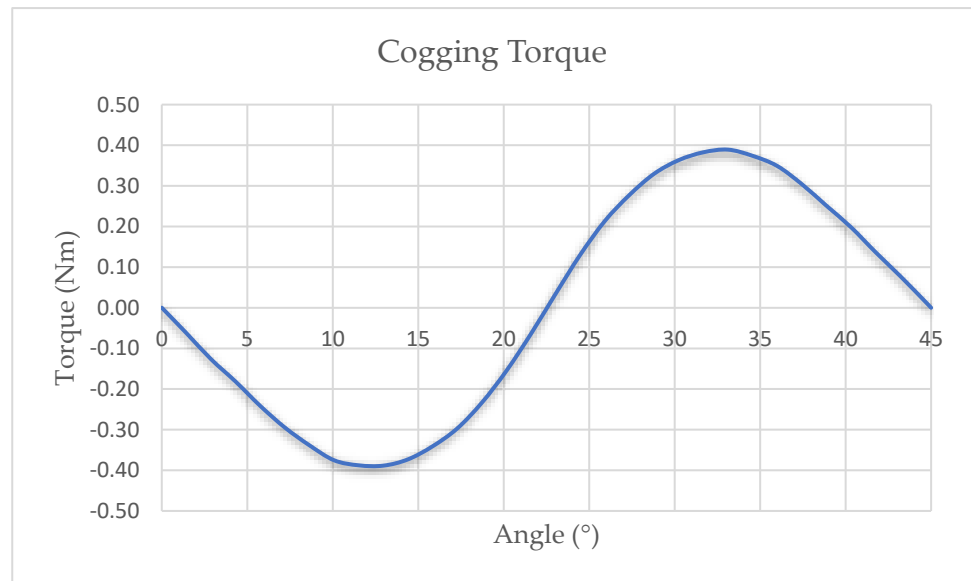


Figure 11. Cogging torque.

The angular period of the cogging torque as per the least common multiple (LCM) based on the number of poles and slots giving 45°. As per the plot, the cogging torque peak is recorded as 0.39 Nm. This torque value could be used to calculate the input force needed to actuate the generator. This is important to understand the extra effort that needs to be applied by the user to occupy the energy harvester device. The perpendicular force at the shaft can be calculated by using Equation (5):

$$F_{\perp} = \tau / \ell \tag{5}$$

where  $F_{\perp}$  is the perpendicular force acting on the shaft in N,  $\tau$  is the torque in Nm and  $\ell$  is the shaft length in meter

Because the cogging torque will influence the required force to actuate the generator, this design is further investigated to reduce the cogging torque. Li Zhu et al. [29] have derived Equations (6)–(8) which demonstrate the direct influence of the slot opening to slot pitch ratio towards the cogging torque.

Equation (6), shows the proportion of cogging torque:

$$T_{\text{cog}}(\alpha_r) \propto - \sum_{n=1}^{\infty} [G_{a_{nNL}} \sin(nN_L \frac{\alpha_p \pi}{N_p}) \sin(nN_L \alpha_r)] \tag{6}$$

Equation (7), shows the direction proportion of cogging torque while the rotor position  $\alpha_r = 2\pi/N_L$ :

$$T_{\text{cog}} \propto \sum_{n=1}^{\infty} T_n = - \sum_{n=1}^{\infty} [G_{a_{nNL}} \sin(nN_L \frac{\alpha_p \pi}{N_p}) \sin(n \frac{\pi}{2})] \tag{7}$$

The Fourier coefficient of the air gap relative permeance  $G(\theta)$  is shown by Equation (8):

$$G_{a_{nNL}} = \frac{2N_s}{\pi} \left[ \int_{\frac{b_0}{2}}^{\frac{\pi}{N_s}} \cos(nN_L \theta) d\theta + \int_0^{\frac{b_0}{2}} \frac{(\frac{h_m}{\mu_r} + gC_{\emptyset})^2 \cos(nN_L \theta)}{[\frac{h_m}{\mu_r} + (g - R_2 + R_2 \cos(\frac{b_0}{2} - \theta)) + \frac{\pi R_2}{2} (\frac{b_0}{2} - \theta)] C_{\emptyset}}^2 d\theta \right] \tag{8}$$

where  $\alpha_r$  is the rotational angle of rotor,  $N_p$  is the number of permanent magnet pole,  $N_s$  is the number of slots,  $N_L$  is the least common multiple between  $N_p$  and  $N_s$ ,  $\alpha_p$  is the effective ratio of pole arc to pole pitch,  $b_0$  is the slot opening,  $h_m$  is the thickness of magnet,  $\mu_r$  is the magnet relative recoil permeability,  $C_{\emptyset}$  is the flux concentration factor,  $g$  is the mechanical air gap,  $R_2$  is the outer radius of air gap and  $G_{a_{nNL}}$  is the Fourier coefficient

of air gap relative permeance. Equations (6)–(8) clearly shows the reduction in the slot opening to slot pitch ratio will reduce the cogging torque.

The slot opening angle and slot pitch angle region in the generator geometry are shown in Figure 12.

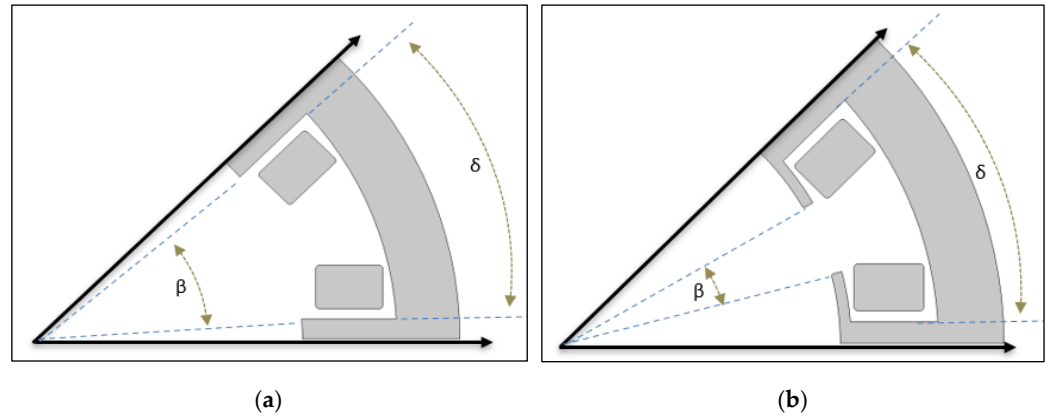


**Figure 12.** Slot opening,  $\beta$  and slot pitch,  $\delta$ . (a) Slot opening for an open slot design. (b) Slot opening for a semi-closed slot design.

The initial generator design has a slot opening to slot pitch ratio of 1 and the geometry of the stator is shown in Figure 12a. To reduce the cogging torque, the  $\beta/\delta$  ratio has been varied by fixing the slot pitch angle to the initial value. Figure 13 shows the cogging torque by  $\beta/\delta$  ratio.

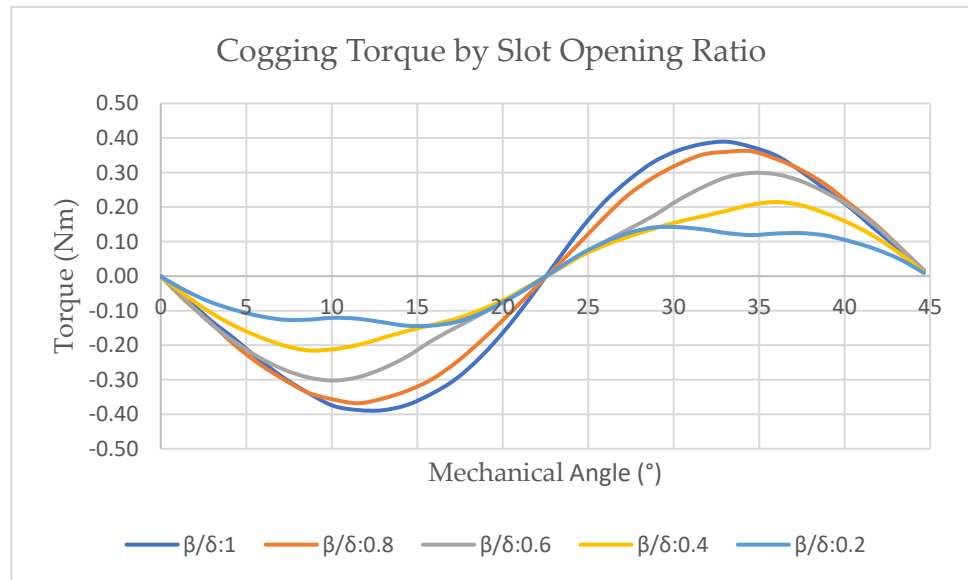


**Figure 13.** Cogging torque by  $\beta/\delta$  ratio.

As expected, the lower  $\beta/\delta$  ratio decreases the cogging torque. The lowest cogging torque, 0.14 Nm, was achieved at a  $\beta/\delta$  ratio of 0.2 but observed a ripple on the cogging torque peak. Hence the  $\beta/\delta$  ratio of 0.4 with cogging torque 0.21 Nm is chosen for this study. This will be 46% lower than the initial cogging torque.

The proposed design has been simulated by varying the parameters as stated in Table 3. The overall simulation outcome has been plotted to illustrate the power generated under two load conditions at different RPM. Figure 14 shows the output power generated at 360 RPM.

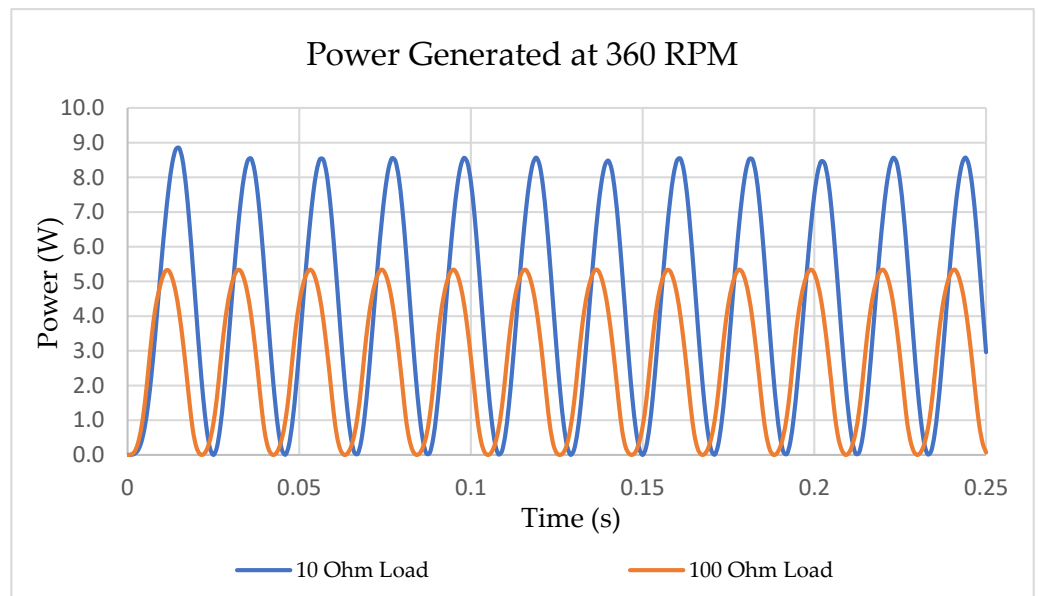


**Figure 14.** Power generated at 360 RPM.

At 360 RPM generator was able to generate a peak power of 8.6 W under a 10-ohm load condition and 5.3 W under a 100-ohm load condition. Figure 15 shows the output power generated at 450 RPM.

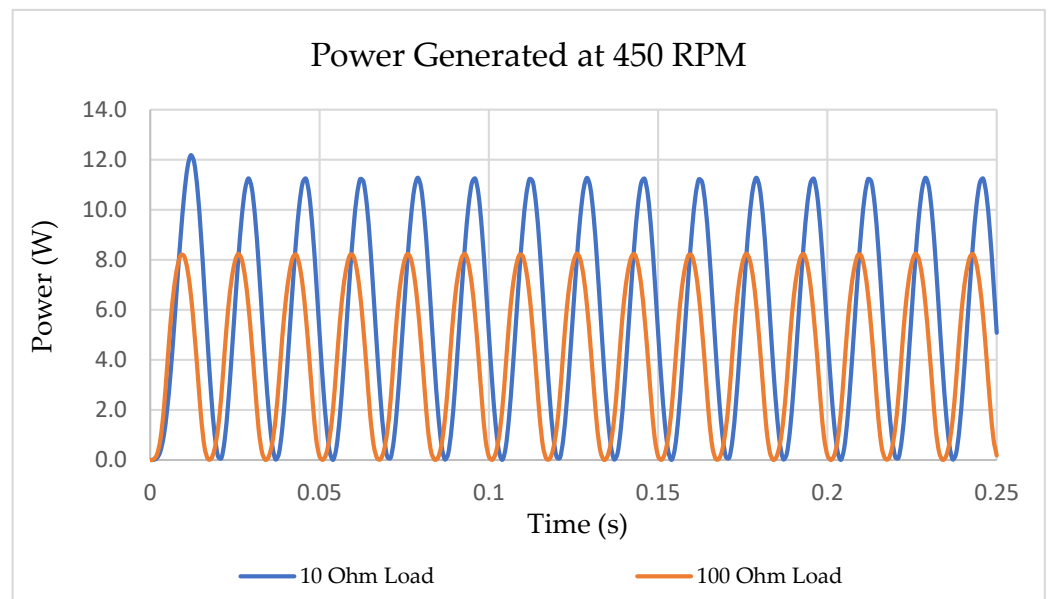


**Figure 15.** Power generated at 450 RPM.

At 450 RPM generator was able to generate a peak power of 11.2 W under a 10-ohm load condition and 8.2 W under a 100-ohm load condition. Figure 16 shows the output power generated at 800 RPM.

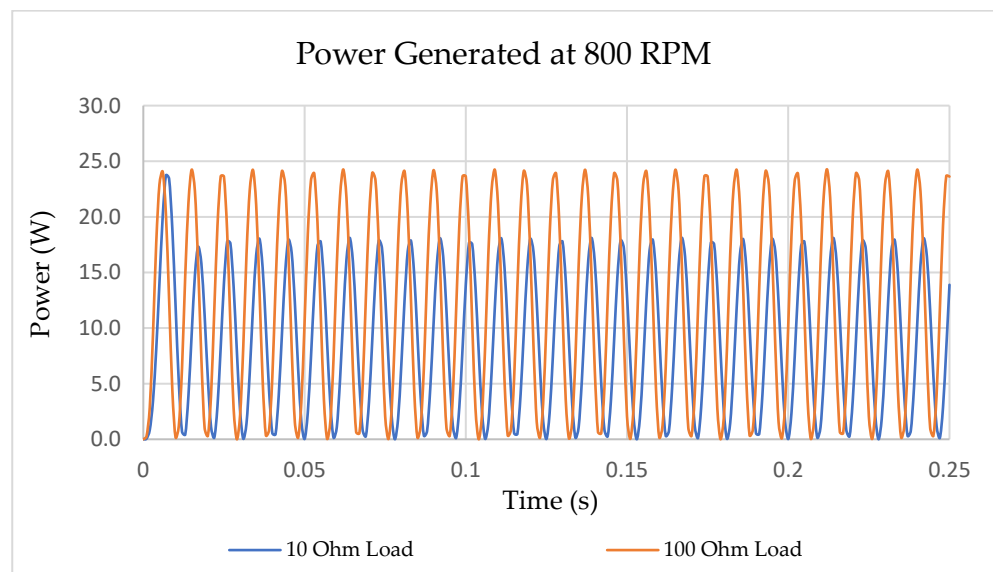


Figure 16. Power generated at 800 RPM.

At 800 RPM generator was able to generate a peak power of 18.1 W under a 10-ohm load condition and 24.2 W under a 100-ohm load condition. The generated output power was further computed to obtain the root mean square value of the power. Figure 17 shows the RMS Power.

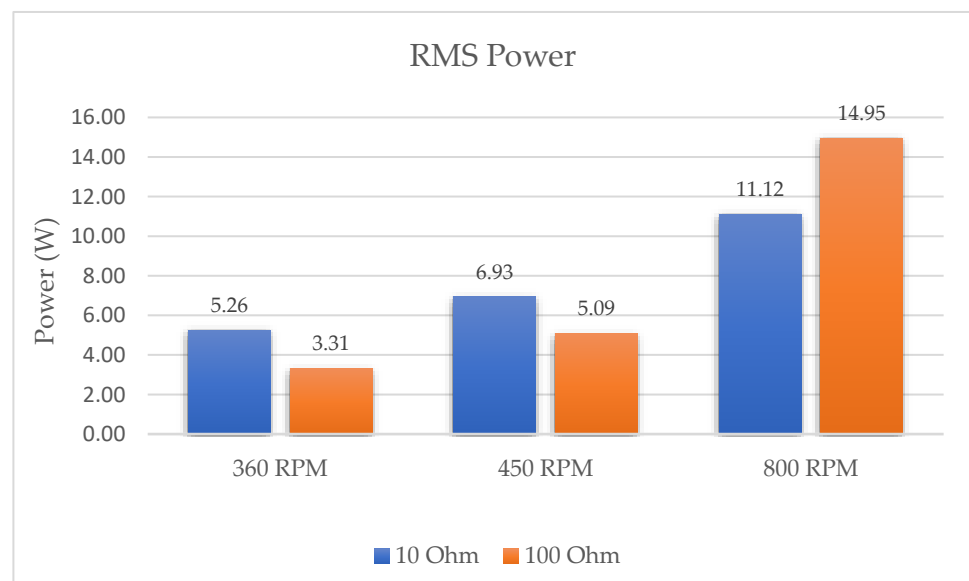
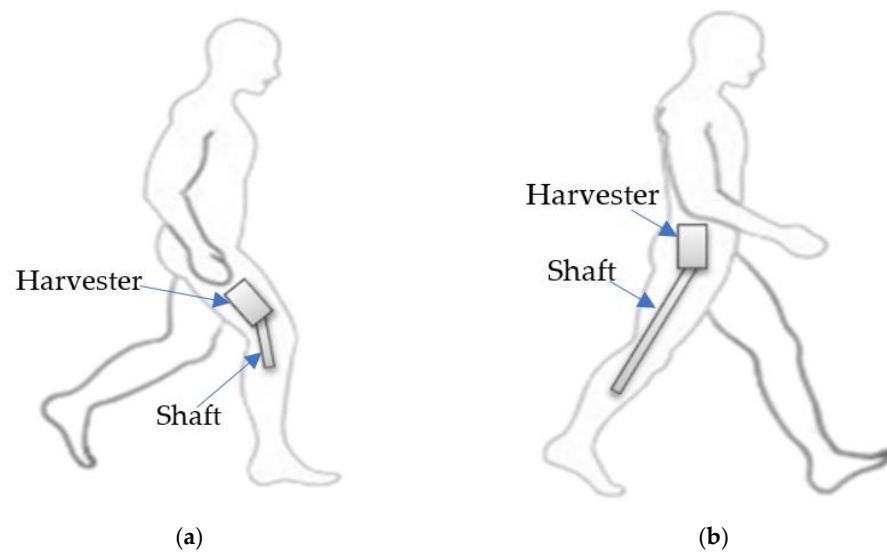


Figure 17. Root mean square power.

The RMS power demonstrates the continuous output power that is able to be supplied by the generator. The minimum RMS power for the generator is 3.31 W with a 100-ohm load at 360 RPM and the maximum RMS power is 14.95 W with a 100-ohm load at 800 RPM.

The overall outcome parameters that have been investigated are analyzed as a case study to summarize the achieved outcome. Figure 18 shows the conceptual image of knee biomechanical energy-harvesting device placement of this electromagnetic generator.



**Figure 18.** Knee biomechanical energy harvester placement. (a) attached to thigh (b) attached to hip.

Case study 1: A male user with a 6-feet 2-inch height walked at 1.34 m/s pace for 30 min by wearing this energy harvester with a 250-mm shaft length. This case study is described in the following steps.

- i. As per Joeeun Ahn et al. [30], the average knee angle transition for one complete gait cycle is  $122^\circ$ , which is equivalent to  $61^\circ$  per step.
- ii. As per Werner et al. [31], a male user with a 6-feet 2-inch height would require 1330 steps to reach a 1-km distance if he walked at 1.34 m/s speed.
- iii. By using the values from steps (i) and (ii), the knee angle transition per second can be computed as:  $\text{knee angle transition} = (1.330 \text{ steps/meter}) \times 1.34 \text{ m/s} \times 61^\circ/\text{step} = 108.83^\circ/\text{s}$
- iv. This knee angle transition can be further amplified by using an integrated gear train mechanism. A gear train with a 1:5:5 ratio is occupied for this computation with the assumption of minimal or neglectable friction. The amplified angle is  $108.83^\circ/\text{s} \times 25^\circ = 2720.75^\circ/\text{s}$ .
- v. The amplified angle of  $2720.75^\circ/\text{s}$  is converted to associated revolutions per minute.  $(2720.75^\circ/\text{s}/360^\circ) \times 60 \text{ s} = 453 \text{ RPM}$ .
- vi. Based on the simulation results, the generator at a rotation speed of 450 RPM is able to generate RMS power of 6.93 W under a 10-ohm load and 5.09 W under a 100-ohm load. This output is based on single device or per leg.
- vii. By using Equation (5), the user needs to apply an input perpendicular force of 0.84 N at the shaft end to actuate the generator and the equivalent energy produced for a 30-min walk will be 6.92 Wh under a 10-ohm load and 5.08 Wh under a 100-ohm load.

Case study 2: A female user with a 5-foot height runs at a 4.47 m/s pace for 30 min by wearing this energy harvester with a 150-mm shaft length. This case study is described in the following steps.

- i. As per Joeeun Ahn et al. [30], the average knee angle transition for one complete gait cycle is  $122^\circ$ , which is equivalent to  $61^\circ$  per step.
- ii. As per Werner et al. [31], a female user with a 5-foot height would require 706 steps to reach a 1-km distance if she runs at 4.47 m/s speed.
- iii. By using the values from steps (i) and (ii), the knee angle transition per second can be computed as  $\text{knee angle transition} = 192.49^\circ/\text{s}$ .
- iv. This knee angle transition can be further amplified by using an integrated gear train mechanism. A gear train with a 1:5:5 ratio is occupied for this computation with the assumption of minimal or neglectable friction. The amplified angle is  $4812.25^\circ/\text{s}$ .

- v. The associated revolution per minute is 802 RPM.
- vi. Based on the simulation results, the generator at a rotation speed of 800 RPM is able to generate RMS power of 11.2 W under a 10-ohm load and 14.95 W under a 100-ohm load. This output is based on single device or per leg.
- vii. By using Equation (5), the user needs to apply an input perpendicular force of 1.4 N at the shaft end to actuate the generator and the equivalent energy produced for a 30-min walk will be 11.2 Wh under a 10-ohm load and 14.96 Wh under a 100-ohm load.

The overall parameters and computed values in the case study are summarized and tabulated in Table 5.

**Table 5.** Summary of case study.

Description	Case Study 1	Case Study 2
User height	6-feet 2-inch	5-feet
Motion speed	1.34 m/s	4.47 m/s
Shaft length	250 mm	150 mm
Steps to reach 1 km	1330 steps	706 steps
Knee angle transition/s	108.83°/s	192.49°/s
Amplified angle	2720.75°/s	4812.25°/s
Associated RPM	450 RPM	800 RPM
RMS power per device with 10-ohm load	6.93 W	11.2 W
Equivalent energy for 30 min	6.92 Wh	11.2 Wh
RMS power per device with 100-ohm load	5.09 W	14.95 W
Equivalent energy for 30 min	5.08 Wh	14.96 Wh
Force applied by the user	0.84 N	1.4 N

As demonstrated in the case study, when the user wears the harvester device on both leg while walking, the user was able to generate RMS power of 13.86 W under a 10-ohm load and 10.18 W under a 100-ohm load by applying minimal input force of 0.84 N by the user. Moreover, while running the user was able to generate RMS power of 22.4 W under a 10-ohm load and 29.9 W under a 100-ohm load by applying 1.4 N force. This case study shows the RMS power generated for walking and running by using the proposed electromagnetic generator design.

In previous work, Feng Qian et al. [22] demonstrated piezoelectric footwear which was able to generate a maximum 8 mW/shoe. Mustafa Ilker et al. [23] designed a knee wearable device that was able to generate a maximum power of 98.5  $\mu$ W while walking and 123.4  $\mu$ W while running. Yiming Lei et al. [24] generated 205.38  $\mu$ W through a microelectromagnetic vibration energy harvester. Muhammad Toyabur Rahman et al. [25] investigated a hybridized generators and were able to generate 131.4 mW. All these power ranges are very minimal as the piezoelectric, triboelectric, and microelectromagnetic harvesters were used as the generators. Longhan Xie et al. [26] harvested 6.47 W at walking speed of 1.41 m/s and Jun Fan et al. [28] were able to generate 4.1 W at 1.5 m/s walking speed, at the lower walking speed of 1.34 m/s minimum RMS power generated in this study was 5.09 W and maximum RMS power generated was 6.93 W. Collier Apgar et al. [27] were able to generate 8.43 W at 5211 RPM, whereby in this study the RMS power generated at 800 RPM was in the range of 11.2 W to 14.95 W. This was comparatively higher power at a lower speed. Maxwell Donelan et al. [20] designed a device that generated  $3.5 \pm 0.35$  W per device at 1.5 m/s walking speed under continuous generation mode. In this study, the RMS power generated at 450 RPM which is associated with a walking speed of 1.34 m/s is 6.93 W and 5.09 W based on the load condition. The significance of this study is exhibited through the output power which is higher compared to the rest of the electromagnetic generator.

#### 4. Conclusions

The study demonstrates the magnet size and stator shape influence the electromagnetic force strength and magnetic flux density at the air gap region. The proposed design exhibits

lower cogging torque which is 0.21 Nm at the 1 mm air gap thickness and this was achieved by reducing the slot opening to slot pitch ratio of the stator design. The generator design was able to produce significantly high power with minimal input perpendicular force to actuate the generator by the user. By applying the force range from 0.84 N to 1.4 N, the user could harvest power between 5.09 W and 14.95 W corresponding to the user's movement speed. This generated power will be doubled when the user wears the biomechanical harvester mechanism on both legs. In future research, the existing design will be evaluated based on the overall harvester mechanism weight and the needed extra effort to carry the harvester device. Moreover, the number of poles and slots will be varied to reduce the generator's weight and the generated output power will be analyzed based on possibilities to compensate by increasing the gear ratio to produce higher RPM. In summary, the biomechanical energy harvester has a substantial opportunity to be a substitute for the conventional battery depending on the application.

**Author Contributions:** Conceptualization, N.G.; Data curation, N.G.; Formal analysis, N.G., I.E. and S.S.; Funding acquisition, I.E.; Investigation, N.G.; Methodology, N.G., I.E., N.Y. and B.-H.T.; Project administration, N.Y.; Resources, N.Y., S.S. and B.-H.T.; Supervision, I.E. and N.Y.; Validation, B.-H.T.; Writing—original draft, N.G.; Writing—review & editing, I.E., N.Y., S.S. and B.-H.T. All authors have read and agreed to the published version of the manuscript.

**Funding:** Funds for this research was provided by Universiti Teknologi PETRONAS (UTP), Malaysia, under research Grant 015LC0-243.

**Institutional Review Board Statement:** Not applicable.

**Informed Consent Statement:** Not applicable.

**Data Availability Statement:** Not applicable.

**Conflicts of Interest:** The authors declare no conflict of interest.

## References

1. Erdiwansyah, M.; Husin, H.; Nasaruddin, M.; Muhibbuddin, A. Critical Review of The Integration of Renewable Energy Sources With Various Technologies. *Prot. Control. Mod. Power Syst.* **2021**, *6*, 3. [CrossRef]
2. Zhou, W.; Du, D.; Cui, Q.; Lu, C.; Wang, Y.; He, Q. Recent Research Progress in Piezoelectric Vibration Energy Harvesting Technology. *Energies* **2022**, *15*, 947. [CrossRef]
3. Masood, F.; Nallagownden, P.; Elamvazuthi, I.; Akhter, J.; Alam, M. A New Approach for Design Optimization and Parametric Analysis of Symmetric Compound Parabolic Concentrator for Photovoltaic Applications. *Sustainability* **2021**, *13*, 4606. [CrossRef]
4. Artyukhov, D.; Gorshkov, N.; Vikulova, M.; Kiselev, N.; Zemtsov, A.; Artyukhov, I. Power Supply of Wireless Sensors Based on Energy Conversion of Separated Gas Flows by Thermoelectrochemical Cells. *Energies* **2022**, *15*, 1256. [CrossRef]
5. Truong, K.H.; Nallagownden, P.; Elamvazuthi, I.; Vo, D.N. An Improved Meta-Heuristic Method to Maximize the Penetration of Distributed Generation in Radial Distribution Networks. *Neural Comput. Appl.* **2020**, *32*, 10159–10181.
6. Kumar, M.; Das, B.; Baloch, M.H.; Nallagownden, P.; Elamvazuthi, I.; Ali, A. Optimal Placement and Sizing of Distributed Generators and Distributed-Static Compensator in Radial Distribution System: Distributed Generators and Distributed-Static Compensator. *Int. J. Energy Optim. Eng.* **2019**, *8*, 47–66. [CrossRef]
7. Truong, K.H.; Nallagownden, P.; Elamvazuthi, I.; Vo, D.N. A Quasi-Oppositional-Chaotic Symbiotic Organisms Search Algorithm for Optimal Allocation of DG in Radial Distribution Networks. *Appl. Soft Comput.* **2020**, *88*, 106067. [CrossRef]
8. Dai, Y.; Bai, Y. Performance Improvement for Building Integrated Photovoltaics in Practice: A Review. *Energies* **2021**, *14*, 178. [CrossRef]
9. Konieczna, A.; Roman, K.; Roman, M.; Śliwiński, D.; Roman, M. Energy Efficiency of Maize Production Technology: Evidence from Polish Farms. *Energies* **2021**, *14*, 170. [CrossRef]
10. Calabrese, B.; Velázquez, R.; Del-Valle-Soto, C.; de Fazio, R.; Giannoccaro, N.I.; Visconti, P. Solar-Powered Deep Learning-Based Recognition System of Daily Used Objects and Human Faces for Assistance of the Visually Impaired. *Energies* **2020**, *13*, 6104. [CrossRef]
11. Niu, P.; Chapman, P. Design and Performance of Linear Biomechanical Energy Conversion Devices. In Proceedings of the 37th Power Electronics Specialist Conference, Jeju, Korea, 18–22 June 2006.
12. BCC Research. Available online: <https://www.bccresearch.com/market-research/energy-and-resources/energy-harvesting-markets-technology-devices-egy097a.html> (accessed on 25 March 2022).
13. BCC Research. Available online: <https://www.bccresearch.com/market-research/energy-and-resources/energy-harvesting-market-technology-devices-egy097b.html> (accessed on 25 March 2022).

14. BCC Research. Available online: <https://www.bccresearch.com/market-research/energy-and-resources/global-markets-technologies-and-devices-for-energy-harvesting.html> (accessed on 25 March 2022).
15. Margaria, R. Positive and negative work performances and their efficiencies in human locomotion. *Int. Z. Angew. Physiol.* **1968**, *25*, 339–351. [[CrossRef](#)] [[PubMed](#)]
16. Paradiso, J.A.; Starner, T. Energy scavenging for mobile and wireless electronics. *IEEE Pervasive Comput.* **2005**, *4*, 18. [[CrossRef](#)]
17. Chapuis, A.; Jaquet, E. *The History of the Self-Winding Watch; 1770–1931 Rolex Watch Co.*: Geneva, Switzerland, 1956.
18. Rome, L.C. Backpack for Harvesting Electrical Energy during Walking and for Minimizing Shoulder Strain. U.S. Patent 6982497B2, 17 March 2004.
19. Rome, L.C.; Flynn, L.; Goldman, E.M.; Yoo, T.D. Generating electricity while walking with loads. *Science* **2005**, *309*, 1725–1728. [[CrossRef](#)] [[PubMed](#)]
20. Donelan, J.M.; Li, Q.; Naing, V.; Hoffer, J.A.; Weber, D.J.; Kuo, A.D. Biomechanical energy harvesting: Generating electricity during walking with minimal user effort. *Science* **2008**, *319*, 807–810. [[CrossRef](#)]
21. Winter, D.A. *Biomechanical and Motor Control of Human Movement*, 3rd ed.; John Wiley and Sons: Hoboken, NJ, USA, 2005.
22. Feng, Q.; Xu, T.-B. Design, optimization, modeling and testing of a piezoelectric footwear energy harvester. *Energy Convers. Manag.* **2018**, *171*, 1352–1364.
23. Beyaz, M.I. Energy Harvesting from Knee Motion Using Piezoelectric Patch Transducers. *Acad. Platf. J. Eng. Sci.* **2019**, *7–2*, 255–260. [[CrossRef](#)]
24. Lei, Y.; Wen, Z.; Chen, L. Simulation and testing of a micro electromagnetic energy harvester for self-powered system. *AIP Adv.* **2014**, *4*, 031303. [[CrossRef](#)]
25. Rahman, M.T.; Rana, S.S.; Salauddin, M.; Maharjan, P.; Bhatta, T.; Park, J.Y. Biomechanical Energy-Driven Hybridized Generator as a Universal Portable Power Source for Smart/Wearable Electronics. *Adv. Energy Mater.* **2020**, *10*, 1903663. [[CrossRef](#)]
26. Longhan, X. An unpowered flexible lower limb exoskeleton: Walking assisting and energy harvesting. *IEEE/ASME Trans. Mechatron.* **2019**, *24*, 2236–2247.
27. Collier, A.; Schmidt, G. Biomechanical Energy Harvesting Using a Knee Mounted Generator. In Proceedings of the IEEE Systems and Information Engineering Design Conference, Charlottesville, VA, USA, 29 April 2016.
28. Fan, J.; Xiong, C.-H. A lightweight biomechanical energy harvester with high power density and low metabolic cost. *Energy Convers. Manag.* **2019**, *195*, 641–649. [[CrossRef](#)]
29. Zhu, L.; Jiang, S.Z. Optimal slot opening in permanent magnet machines for minimum cogging torque. *Przeglad Elektrotechniczny* **2011**, *87*, 3.
30. Ahn, J.; Hogan, N. Walking is not like reaching: Evidence from periodic mechanical perturbations. *PLoS ONE* **2012**, *7*, e31767. [[CrossRef](#)] [[PubMed](#)]
31. Werner, W.K.; Bond, L.; Ransdell, L. One-Mile step count at walking and running speeds. *ACSM Health Fit. J.* **2008**, *12*, 14–19.